RESEARCH ARTICLE

WILEY

Seasonal water storage and release dynamics of *bofedal* wetlands in the Central Andes

Anthony C. Ross[1] | Marc Martinez Mendoza[1] | Fabian Drenkhan[2] |
Nilton Montoya[3] | Jan R. Baiker[4] | Jonathan D. Mackay[5,6] |
David M. Hannah[6] | Wouter Buytaert[1,7]

[1]Civil and Environmental Engineering, Imperial College London, London, UK

[2]Geography and the Environment, Department of Humanities, Pontificia Universidad Católica del Perú (PUCP), Lima, Peru

[3]Departamento Académico de Agricultura, Universidad Nacional de San Antonio Abad del Cusco (UNSAAC), Cusco, Peru

[4]Asociación para la Conservación y Estudio de Montañas Andinas-Amazónicas (ACEMAA), Cusco, Peru

[5]British Geological Survey, Environmental Science Centre, Keyworth, UK

[6]School of Geography, Earth and Environmental Sciences, University of Birmingham, Edgbaston, UK

[7]Grantham Institute – Climate Change and the Environment, Imperial College London, London, UK

Correspondence
Anthony C. Ross, Civil and Environmental Engineering, Imperial College London, London, UK.
Email: ar3220@ic.ac.uk

Abstract

Tropical high-Andean wetlands, locally known as 'bofedales', are key ecosystems sustaining biodiversity, carbon sequestration, water provision and livestock farming. Bofedales' contribution to dry season baseflows and sustaining water quality is crucial for downstream water security. The sensitivity of bofedales to climatic and anthropogenic disturbances is therefore of growing concern for watershed management. This study aims to understand seasonal water storage and release characteristics of bofedales by combining remote sensing analysis and ground-based monitoring for the wet and dry seasons of late 2019 to early 2021, using the glacierised Vilcanota-Urubamba basin (Southern Peru) as a case study. A network of five ultrasound loggers was installed to obtain discharge and water table data from bofedal sites across two headwater catchments. The seasonal extent of bofedales was mapped by applying a supervised machine learning model using Random Forest on imagery from Sentinel-2 and NASADEM. We identified high seasonal variability in bofedal area with a total of 3.5% and 10.6% of each catchment area, respectively, at the end of the dry season (2020), which increased to 15.1% and 16.9%, respectively, at the end of the following wet season (2021). The hydrological observations and bofedal maps were combined into a hydrological conceptual model to estimate the storage and release characteristics of the bofedales, and their contribution to runoff at the catchment scale. Estimated lag times between 1 and 32 days indicate a prolonged bofedal flow contribution throughout the dry season (about 74% of total flow). Thus, our results suggest that bofedales provide substantial contribution to dry season baseflow, water flow regulation and storage. These findings highlight the importance of including bofedales in local water management strategies and adaptation interventions including nature-based solutions that seek to support long-term water security in seasonally dry and rapidly changing Andean catchments.

KEYWORDS
bofedales, high-altitude wetlands, random forest, residence time, seasonal buffering, supervised classification, tropical Andes, Vilcanota headwaters, water security

1 | INTRODUCTION

In the Southern Tropical Andes, high-altitude wetlands are a characteristic feature of the mountain hydrology. They are locally known as 'bofedales' or 'oconales' (Chimner et al., 2019; Gandarillas et al., 2016; Garcia & Otto, 2015) and cover most parts of Central and Southern Peru, Bolivia, Northern Chile and Argentina at an altitudinal range of about 3500–5200 m asl (García & Beck, 2006; Meneses et al., 2019; Otto et al., 2011; Squeo et al., 2006). These ecosystems are characterized for being remarkably exposed to extreme conditions, such as strong winds, diurnal thermal contrasts, pronounced dry seasons, high solar radiation, and low oxygen concentrations (Gandarillas et al., 2016; Squeo et al., 2006). Bofedales are known to be high primary production systems of seasonally dry and moist habitats (Buitrón-Aliaga & Fernández-Callisaya, 2012), typically located on flat or slightly inclined (from 0 to 15°) fluvial and glacial valleys, alluvial plains and fluvial terraces (Garcia Dulanto, 2018; Mango-Mamani, 2017). They develop over colluvial deposits or plane surfaces, such as lacustrine plains, or filled shallow pits, such as fluvio-glacial kettles or bed-rock potholes (Squeo et al., 2006) and are inhabited by a diverse set of low-growing hydrophytic plants that often accumulate peat and are occasionally accompanied by herbaceous vegetation between 0.1 and 0.5 m tall (MINAM, 2019).

Bofedales provide essential ecosystem services including water provision, biodiversity and carbon sequestration (Maldonado Fonkén, 2014; Mango-Mamani, 2017; Miguel et al., 2012; Monge-Salazar et al., 2022; Polk et al., 2017; Yager et al., 2019). They are also an essential part of the Andean indigenous heritage and culture, including their traditions, economic activities, recreation, landscape aesthetics and spiritualism (Alcántara-Boñón, 2014; Mango-Mamani, 2017; White-Nockleby et al., 2021). However, bofedales are sensitive to environmental changes (Anderson et al., 2021; Dangles et al., 2017; Earle et al., 2003; Otto & Gibbons, 2017) and thus particularly vulnerable to human disturbances including climate change and land-use or land cover changes (Polk et al., 2017). In the last decades, overgrazing, drainage, peat extraction, soil loss, and road construction have been major causes of bofedal degradation (Gandarillas et al., 2016; Maldonado Fonkén, 2014). Climate change is expected to alter the hydrology, productivity and spatial distribution of individual wetland ecosystems, due to shifts in precipitation and thermal regimes (Anderson et al., 2021; Erwin, 2008; Otto & Gibbons, 2017). Increasing drought conditions in the region (Castellanos et al., 2022; Neukom et al., 2015) will affect water inputs and evapotranspiration, while increasingly intense rainfall events (Castellanos et al., 2022) may increase rates of erosion that can contribute to wetland habitat degradation or loss (Seneviratne et al., 2012).

Generating a well-founded understanding of high-Andean hydrology, including in wetland dominated regions, has been difficult due to a strong lack of resources and hydrometeorological monitoring. Findings are fragmented as catchment features (i.e., glaciers, wetlands and groundwater) tend to be researched in isolation (Navarro et al., 2023). Few studies have aimed to characterize the role of bofedales in catchment hydrology (Cooper et al., 2019; Polk et al., 2017; Valois

et al., 2020; Valois et al., 2021), however, findings are widespread and somewhat inconsistent. Furthermore, no attempts have been made to quantify their relative streamflow contribution or seasonal buffering capacity. This evidence would be paramount in building an understanding of how bofedales will respond to changes in climate and human intervention and, therefore, how future downstream water supply might be affected. This lack of hydrological characterization combined with the vulnerability of bofedales to human disturbance and environmental change, and their importance for local and regional water supply, poses severe challenges to their sustainable management (e.g., Drenkhan et al., 2023). In this context, using the headwaters of the Vilcanota-Urubamba basin (Southern Peru) as a case study, we provide a framework to quantify the seasonal water storage and release dynamics of bofedales using minimal monitoring and widely available data. This study aims to: (1) understand the spatio-temporal dynamics of bofedales extent by mapping them in respective wet and dry seasons, and (2) estimate the streamflow contribution of bofedales relative to other catchment features, using a novel combination of in situ measurements, analysis of remotely sensed data, and hydrological modelling.

2 | METHODS

2.1 | Study region

Our study catchments are located within the Vilcanota-Urubamba basin (VUB) in Southern Peru in the transition area of the wet Puna grassland and steppe ecoregion (Squeo et al., 2006) in the south and the tropical rainforests in the north of the basin (Figure 1). The VUB covers a surface area of 11 052 km^2 and an elevation range from about 1100 to 6300 m asl (Figure 1a,b). It is a glacierised basin with total glacier area of 142 km^2 (Drenkhan et al., 2018). Our study focuses on the Sibina Sallma (41.6 km^2) and Halairipampa (54.1 km^2) catchments (Figure 1c) in the high wet Puna region in the southeastern part of the VUB. Halairipampa includes a large glacier coverage (about 8.9 km^2), whereas glacier extent in Sibina Sallma is very limited (<0.1 km^2).

Two weather stations are in the vicinity of the studied catchments: Sibinacocha Lake and Quelccaya Glacier (4880 and 5650 m asl, respectively; Figure 1c). Sibinacocha indicates 776 mm/year precipitation on average (2017–2021) from which 66% (511 mm) occurred during the wet season (December–March) and 4% (29 mm) during the dry season (June–August). Average annual precipitation at Quelccaya was 1199 mm/year (2016–2020) from which 60% (718 mm) occurred during the wet season and 7% (79 mm) during the dry season. Annual average surface temperature at Sibinacocha varied between 2.6°C in austral wet summer (December–March) and 1.0°C in austral dry winter (June–August).

Exposed bedrock on the Sibina Sallma valley slopes is dominated by the Devonian metapelitic Cabanillas group which is locally overlain by the younger volcano-sedimentary Mitu group to the south. The Halairipampa catchment bedrock is dominated by the Carboniferous
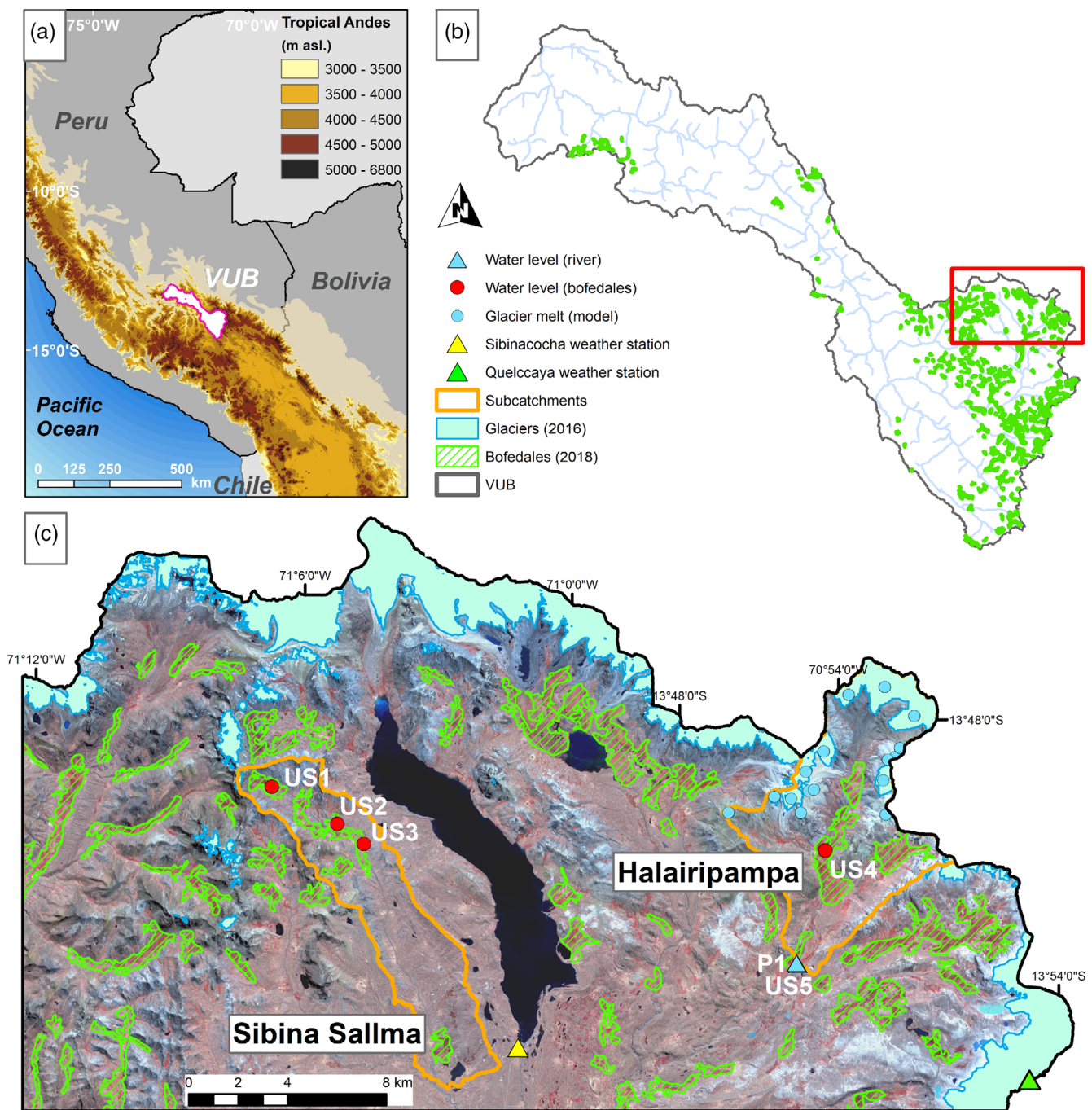
FIGURE 1 Location of the Vilcanota-Urubamba basin (VUB) within Peru (a), map of the VUB (b) and map of the Sibina Sallma and Halairipampa catchments within the VUB (c).

Ambo (sandstone) Group. The bofedales in both catchments are almost exclusively constrained to the valley floors where they overlie extensive, highly permeable glacio-fluvial and alluvial deposits. They typically comprise a high-permeability organic peat layer underlain by clay-rich lacustrine deposit. This low permeability horizon likely promotes the formation of the bofedales by inhibiting surface drainage to the buried unconsolidated deposits beneath (Glas et al., 2018).

Total bofedal cover for Peru has been estimated by the Peruvian Ministry of Environment (MINAM) within the national ecosystem inventory with a baseline for 2016. According to this assessment, the Sibina Sallma catchment covers a bofedal area of 3.8 km^2 (9.1%) while Halairipampa includes 5.8 km^2 (10.7%), bofedal area over the VUB is 267.4 km^2 (2.4%) and 5481.7 km^2 (0.4%) for Peru (MINAM, 2019). This inventory, partially based on remote sensing data and only considering larger bofedal areas (minimum = 20 ha), has important limitations as total bofedal area may highly depend on seasonal variability, and the considered thresholds and model accuracy (UNEP, 2022).

2.2 | Seasonal bofedales extent mapping

Bofedales is a local term used across the Southern Tropical Andes that does not yet have a formal definition. For example, in some literature, bofedales are considered peatlands (e.g., Valois et al., 2020; Valois et al., 2021). However, we have adapted a version of the definition given in Maldonado Fonkén (2014) to areas of land that are saturated for a sufficient period during the year to sustain various types of high-altitude wetland plant communities. The underlying soil may or may not have the presence of peat, they can be seasonally or permanently saturated and natural or man-made. Therefore, our classification model aims to capture all high-altitude wetlands within the study region, including but not limited to peatlands. The model was used to map bofedales extent in the dry and the wet season. However, we do not assume that actual bofedal area changes seasonally but, rather, that the resulting maps give an indication to the seasonal differences in bofedal water storage.

Bofedales extent for the VUB was mapped using multi-spectral Sentinel 2 observations. This dataset is particularly suited for vegetation analysis because it includes a near-infrared band at 10 m as well as three red-edge bands and two short-wave infrared bands at 20 m spatial resolution (Gatti & Bertolini, 2015). We acquired Sentinel 2 observations for the end of the dry (01/08/2020–30/11/2020) and wet (01/04/2021–14/06/2021) seasons. Images were filtered by pixel-wise cloud cover probability >10%, then mosaicked into cloud-free images for each season using median band values (Shepherd et al., 2020).

Next, we applied supervised classification using the Random Forest (RF) machine learning algorithm. This method has been proven to provide uniform and high accuracy results when applied over large areas (Mutanga & Kumar, 2019) and has been successfully applied to map tropical high-Andean wetlands (cf. Chimner et al., 2019; Hribljan et al., 2017; Jara et al., 2019). RF uses bootstrap aggregation (bagging) to generate an ensemble of 'trees' in which each classifier is trained on a random subspace of features (Belgiu & Drăguţ, 2016). Once trained, the final prediction is obtained by a majority voting system of each model from the ensemble (Ham et al., 2005; Mutanga & Kumar, 2019).

A major benefit of the RF method is the ability to incorporate co-variables to improve the classification (Belgiu & Drăguţ, 2016; Ham et al., 2005). Here, we used a total of 20 vegetation and 7 topographic indices (Appendix A, Tables A1, A2) that potentially enhance the spectral differentiation of vegetation from satellite imagery to identify potential bofedales extent (Jara et al., 2019; Mahdavi et al., 2018). Topographic indices were derived from the NASADEM dataset, which has a 30 m spatial resolution (Buckley et al., 2020).

In absence of ground-validated data on land cover types within the study area, a training point sampling strategy was developed using two Regions of Interest of clearly identifiable bofedal and non-bofedal areas. Therefore, iteratively determined thresholds were defined based on a scoping literature review using the three most common vegetation and topographic indices for wetland classification for both the dry and wet season (Appendix A, Tables A3–A5).

A stratified random sampling method was applied to the resulting two Regions of Interest to reduce the accuracy estimation errors of non-abundant features (i.e., bofedal pixels) and to increase the number of samples to improve the accuracy of the model without biasing the performance estimators (Olofsson et al., 2014). The sampling size necessary to achieve a target standard error was calculated following Cochran (1977). The RF model was then refined to reduce overfitting (Appendix A, Random Forest (RF) model refinement).

To evaluate model performance, a binary confusion matrix was generated based on the Matheus Correlation Coefficient (Chicco et al., 2021), sensitivity and accuracy (Starovoitov & Golub, 2020) performance assessments. Lastly, three postprocessing steps were applied to reduce residual errors. The first two were adopted in Baum & Zanetti (2015), Kumar (2020) and Mohammadi et al. (2020): (i) eliminating bofedal pixels if less than half of their eight neighbour pixels were considered bofedales and (ii) eliminating bofedal areas less than 3 × 3 pixels. Pixel resolution is attributed to the 30 m resolution NASADEM input data. The outcome resolution encompasses a minimum of 3 × 3 pixels (0.8 ha) necessary in determining a category to map. This resolution has been shown to be effective to identify vegetation (Li et al., 2021; Shamsoddini & Raval, 2018) and, specifically, bofedales (Garcia Dulanto, 2018; García & Lleellish, 2012). The final postprocessing step, (iii) a water mask based on the Normalized Difference Water Index was applied to avoid confusion of bofedales with lakes and other open water bodies.

2.3 | Hydrometeorological data collection and processing

Groundwater observation boreholes of 0.15 m diameter were installed at depths between 1.1 and 2.5 m in four representative bofedal locations across the two catchments (US1-4, Figure 1; Table 1). For boreholes US2 and US3, total borehole depth was limited upon reaching hard clay lacustrine material where manual core extraction was not feasible. Afterwards, the borehole was widened to allow the insertion of perforated pipes. The pipes were capped with a PVC lid onto which a downward-facing ultrasound water level logger was installed. An additional ultrasound logger (US5) was fitted at the outlet of the Halairipampa catchment to measure river levels. At this location, previous water level data from a pressure transducer (P1) are also available. The records between US5 and P1 showed good agreement for the overlapping period and, therefore, they were merged into a single time series of water level.
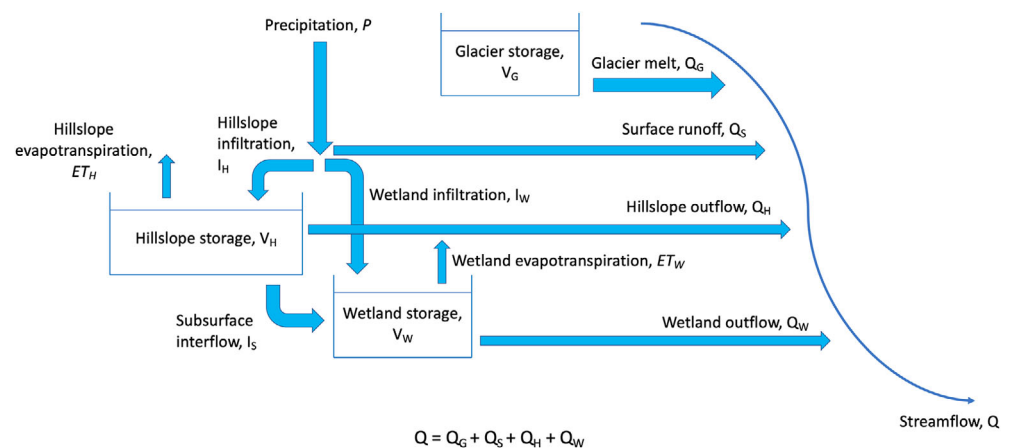
US1-5 recorded data at a 5-min interval (P1 at a 30-min interval). The measurements were datum-adjusted and smoothed using a moving average with a window of 30 min to reduce noise. These were averaged to daily frequency to minimize the impact of the diurnal temperature cycle in these data. This is caused by temperature variations in the air column of the pipe, which are exceptionally high in tropical mountain regions and affect ultrasound wave transmission. Three manual flow estimations were made between October 2016 and December 2018 at the outlet of the Halairipampa catchment

TABLE 1 Characteristics of the hydrological loggers used for this study in the two sub-catchments Sibina Sallma and Halairipampa.

Sibina Sallma				Halairipampa			
Logger	Coordinates	Altitude	Period	Logger	Coordinates	Altitude	Period
US1	13°49′43″S 71°06′41″W	5045 m asl	11/2019–03/2021	US4	13°50′55″S 70°54′14″W	4813 m asl	11/2019–03/2021
US2	13°50′31″S 71°05′12″W	4930 m asl	11/2019–04/2021	US5	13°53′25″S 70°54′49″W	4757 m asl	11/2019–03/2021
US3	13°50′56″S 71°04′36″W	4912 m asl	11/2019–12/2021	P1	13°53′25″S 70°54′49″W	4757 m asl	08/2016–12/2020

Note: US1–US4, ultrasound water level loggers installed in the bofedales; US5, ultrasound water level logger to measure river stage; P1, pressure transducer to measure river stage. Borehole logs are available in Appendix B, Table B1.

FIGURE 2 Conceptual model of the hydrology of high-altitude wetland dominated headwater catchments to disaggregate the contribution of different end members (glacier melt Q_G, surface runoff Q_s, hillslope outflow Q_H, and wetland outflow Q_W) to total streamflow (Q).

using float gauging. A power law was fitted to the data points to formulate a rating curve. The resulting discharge hydrograph was separated into stormflow and baseflow following Gustard et al. (1992). We assume that all stormflow is produced by surface runoff due to the velocity of the response.

The Sibina Sallma and Halairipampa catchments were delineated using the D8 flow direction algorithm on the unsampled SRTM-based ALOS PALSAR DEM at 12.5 m. These catchment boundaries were used to crop the VUB bofedales extent maps to derive the wet and dry season extent for each catchment. A time series of bofedales extent in Halairipampa was produced by interpolating between the dry and wet season extents, assuming a linear relation with the water levels at US4. The nearest precipitation data were obtained from the Sibinacocha and Quelccaya weather stations (Figure 1c).

2.4 | Hydrological analysis

2.4.1 | Catchment hydrological model

Here, we build a catchment-scale hydrological model to understand and quantify the temporal dynamics of streamflow contributions from different sources (end members). This model is based on a review of available and relevant literature on Andean and other wetland-dominated catchments with similar behaviour (Cooper et al., 2019;

Lazo et al., 2019; Mosquera et al., 2016; Soulsby et al., 2009). Based on these studies we identify direct surface runoff (Q_s), glacier melt (Q_G), shallow subsurface runoff from hillslopes (Q_H), and wetland subsurface flow (Q_w) as main streamflow contributions (Figure 2). Mosquera et al. (2016) and Rodríguez-Morales et al. (2019) show that deep groundwater contributions to hillslope or wetland recharge and streamflow are often negligible in high mountain conditions. This may not be the case in our catchment because of the presence of proglacial moraine deposits which act as groundwater stores (Somers & McKenzie, 2020). However, it is a conservative assumption because it will lead to an underestimation of the catchment's hydrological buffering capacity.

Conceptual models to estimate each of these flows from our observations are outlined in the next subsections. Because of a lack of reliable radiation data, we estimated evapotranspiration by closing the catchment water balance using precipitation and discharge data. Lastly, it is worth pointing out that isotope analysis by Cooper et al. (2019) found that streamflow and glacier melt contributions to hillslope or wetland recharge in this region were negligible. Therefore, both are modelled as parallel and independent flow pathways.

We apply our model to the Halairipampa catchment, since only discharge data for this catchment were available. Resolving the catchment water balance for the 16-month study period using the Sibinacocha rainfall data, we found a runoff ratio of 1.00 for Halairipampa, with total rainfall and runoff equal to 1371 mm. This is unrealistically

high and indicates errors in the water balance. We attribute this error to the location of the Sibinacocha meteorological station, which is southwest of the Halairipampa catchment. A strong northeast-southwest gradient of decreasing precipitation is present in the region because of moisture spill-over from the Amazon basin. The Quelccaya rainfall data, which gave a runoff ratio of 0.897 for the studied period, were used as the driving input to the model. The runoff ratio is still unrealistically high; however, our interests are in the relative stream-flow contributions of end members and their temporal dynamics, rather than predicting flow magnitudes. As such, we did not apply a correction factor.

2.4.2 | Glacial melt (Q_G)

Glacial melt contribution was simulated using the glacier component of the Joint UK Land Environment Simulator (JULES). JULES solves the energy balance of glacier ice and snow and has been used to estimate glacier meltwater runoff (Shannon et al., 2019). The use of JULES over simpler temperature-based melt models is important as it can simulate both sublimation and ablation processes which bring about highly non-linear response to climate variability in high-altitude tropical mountains (Fyffe et al., 2021).

The JULES mass balance simulations were used to drive the physically based Open Global Glacier Model (OGGM) ice flow model (Maussion et al., 2019) which solves the shallow ice equation to determine changes in glacier volume and surface area over time. Meltwater runoff simulations 2000–2018 were produced for a total of 16 glaciers covering 10.8 km^2 of the study area. A subsequent analysis against geodetic mass balance data (Dussaillant et al., 2019) were used to identify any bias in the simulated glacier mass changes between 2000 and 2018. The meltwater runoff simulations were then bias-corrected to best-replicate the actual glacier streamflow.

Because of a lack of input data for the studied period, the annual cycle of discharge from glacier melt was calculated. A 28-day moving average was used to smooth the data and obtain a seasonal response before taking the average of the previously modelled period (2000–2016). The error is considered low because of the consistent annual pattern of glacier melt.

2.4.3 | Surface runoff (Q_S)

Studies suggest that surface runoff production in high-Andean catchments is predominantly caused by saturation excess rather than infiltration excess (Buytaert & Beven, 2011; Lazo et al., 2019; Mosquera et al., 2015; Mosquera et al., 2016). Therefore, we posited a direct linear relation between bofedales extent and surface runoff production in the catchment. However, a linear regression between the monthly surface runoff percentage of rainfall and the monthly average areal bofedales extent gave a weak negative correlation (p-value = 0.823). Therefore, a constant factor (total surface runoff over total

precipitation) was used to simulate daily surface runoff as a fraction of precipitation.

2.4.4 | Shallow subsurface runoff (Q_{W+H})

Previous studies have shown that the subsurface runoff of high-Andean wetland catchments behaves as a set of parallel linear reservoirs with different residence times (Buytaert et al., 2004; Buytaert & Beven, 2011). Here we combine this linear reservoir behaviour with the observational data from the water level sensors to build a conceptual model of the shallow subsurface runoff. We model Q_W and Q_H jointly as Q_{W+H} because hillslopes often feed into wetlands and our experimental approach does not allow separation of the fluxes. A linear reservoir is characterized by the equation:

$$Q_{W+H} = kS \tag{1}$$

where Q is the outflow of the wetlands, k is the linear reservoir drainage rate coefficient (rate constant) and S is the total storage capacity of the wetlands and hillslopes. If we assume that wetland storage is much larger than hillslope storage and that there is a linear relation between the wetland extent and the storage capacity, then S can be represented as:

$$S = h \cdot A_d + \frac{h(A_w - A_d)}{H} \tag{2}$$

where A_w is the maximum wetland extent during the wet season, A_d is the minimum wetland extent during the dry season, h is the water level of the wetland above the seasonal minimum, and H is the maximum level difference between A_d and A_w. Combining both formulas yields:

$$Q_{W+H} = k \cdot h \cdot A_d + \frac{h(A_w - A_d)}{H} \tag{3}$$

Which yields a linear relation between Q_{W+H} and h. While it would be possible to use the linear reservoir model directly to estimate Q_{W+H} based on h, this does not allow explicit representation of the response delay between the precipitation event and the peak of the wetland flow. This delay may be substantial because many wetlands are fed by shallow hillslope flow from upslope contributing areas in addition to direct surface runoff.

Therefore, we estimate instead the unit hydrograph of each bofedales' outflow. The linear relation between Q and h (Equation 3) means that the shape of the stage hydrograph and the flow hydrograph only differ by a scaling factor. From this follows that the stage time series can be used to derive the unit hydrograph, as it is scaled for unit volume anyway. Here we use the distribution of Nash (1957) (Equation 4):

$$u = \frac{v}{k \cdot \Gamma(n)} \cdot e^{-\frac{t}{k}} \cdot \left(\frac{t}{k}\right)^{n-1} \tag{4}$$

where u = unit hydrograph ordinate, v = volume of direct runoff, t = time, k = parameter with dimension of time, n = dimensionless parameter and Γ = gamma function.

First, the lag time between precipitation input and the unit hydrograph peak was determined by maximizing the cross-correlation between rainfall and subsurface water levels (Cooper et al., 2019). Lag times for bofedales in the Sibina Sallma catchment were calculated using data from the Sibinacocha weather station, based on their proximity, whereas lag times for Halairipampa were calculated using data from the Quelccaya weather station (Figure 1c). During the dry season, levels at US3 fall below the depth of the well, therefore, this section of the data was removed from the cross-correlation analysis. A smoothing spline was applied to the US2 and US4 cross-correlation plots to reduce noise.

For the rising limb, a linear increase to the peak was assumed. For the falling limb, respective sections of the observed recession curve during the dry season, least disturbed by precipitation, were used (Appendix C, Table C1). These were extended linearly to a point of zero flow and the results were normalized to unit volume. The Nash (1957) distribution was fitted to these unit hydrographs using the Nelder–Mead algorithm (Nelder & Mead, 1965) to minimize the root-mean-square error (RMSE) with the Nash (1957) parameters k and n, and the point of zero flow as free parameters. Since the US2 and US4 unit hydrographs showed high resemblance, a combined unit hydrograph was fitted to the data from both locations. This resulted in 3 unit hydrographs. As we selected representative points in the landscape, we assume that these jointly represent the bofedales behaviour at the catchment scale.

Subsequently, to estimate the relative contribution of each of those hydrographs to the catchment flow, we introduce partitioning constants to weigh each hydrograph, such that:

$$Q_{W+H} = \sum_{i=1}^{3} w_i \, P * U_i \tag{5}$$

where P is the precipitation time series, U_i are the unit hydrographs, * is the convolution operator, and w_i are the partitioning constants, which are greater than 0 and sum to 1.

The values for these partitioning constants were estimated by minimizing the RMSE between the observed subsurface flow (baseflow minus glacial melt) and modelled subsurface flow, again using the Nelder–Mead algorithm (Nelder & Mead, 1965). There is a distinct reduction in the Quelccaya 2020–2021 wet season rainfall which is not reflected in the Halairipampa hydrograph. Therefore, we fitted the modelled subsurface flow to the observed 2019–2020 wet season and following dry season subsurface flow (until 11/08/2020).

Lastly, we assume that the outflow of the bofedales contributes directly to river discharge without any further delay, for example by passing through groundwater storage. This is a conservative assumption because it will likely lead to an underestimation of the bofedales' buffering capacity.

3 | RESULTS AND DISCUSSION

3.1 | Bofedales extent

The supervised classification using the RF algorithm reveals a total bofedal area of 1.4 km^2 and 6.3 km^2 for the Sibina Sallma and Halairipampa catchments, respectively, during the dry season (2020). During the wet season (2021) we find total areas of 6.3 km^2 for Sibina Sallma and 9.1 km^2 for Halairipampa. These values highlight the strong variability of bofedal occurrence during the dry (wet) season with a total catchment share of 3.5% (15.1%) and 10.6% (16.9%) for Sibina Sallma and Halairipampa, respectively (Figure 3). At the VUB level, a total bofedal area of 282.3 km^2 (630.0 km^2) was identified for the dry (wet) season, amounting to 2.6% (5.7%) of the entire basin area. As mentioned in the methods, we do not infer that actual bofedal area changes seasonally but that these results, rather, indicate seasonal differences in bofedal water storage. If we assume that full bofedales extent is captured during the wet season, then compared to the MINAM (2019) inventory, our model captures over double the bofedal area within the VUB. This is mainly attributed to the capacity of our model to capture smaller bofedales due to the higher resolution of 0.8 ha compared to 20 ha in MINAM (2019). Without ground truthing, however, we cannot rule out that our results may overestimate bofedal area.

The performance assessment of the cross-validation revealed a high Matheus Correlation Coefficient of 0.91 for the dry season and 0.93 for the wet season, meaning that most of the classified zones were attributed to their correlation with the input variables rather than randomness. The sensitivity of the models to bofedales was 0.95 for both seasons, which indicates that the majority of bofedales were detected by the model. The accuracy of the model was 0.96 and 0.97 in the dry and wet season models, respectively. These values indicate a high correlation between the predicted outputs and the validation samples.

Our results show a higher area fraction of bofedales in the glacier fed Halairipampa catchment, but a less pronounced seasonal variation (a wet/dry season ratio of 1.6) compared to the Sibina Sallma catchment (ratio: 4.4). This is probably the result of different topography, as the Halairipampa catchment has more extensive overlain layers of low-permeable ground and high-permeable surface deposit, which in combination with upslope dry-season water inputs favour bofedal development. However, we cannot exclude that glacier inputs may further enhance this process (cf. Polk et al., 2017).

For the entire VUB, bofedales occur predominantly in high-elevated Vilcanota mountain range around Sibina Sallma and Halairipampa, which is most likely related to its diverse geomorphological setting, including flood plains, valley bottoms and flat surfaces. In the north-western part of the VUB, bofedales occurrence is much more limited, which can probably be attributed to topography and a limited number of flat areas (cf. Drenkhan et al., 2018). Seasonal variations of bofedales are far more pronounced around Lake Sibinacocha. In this area, high variability of interannual wetting
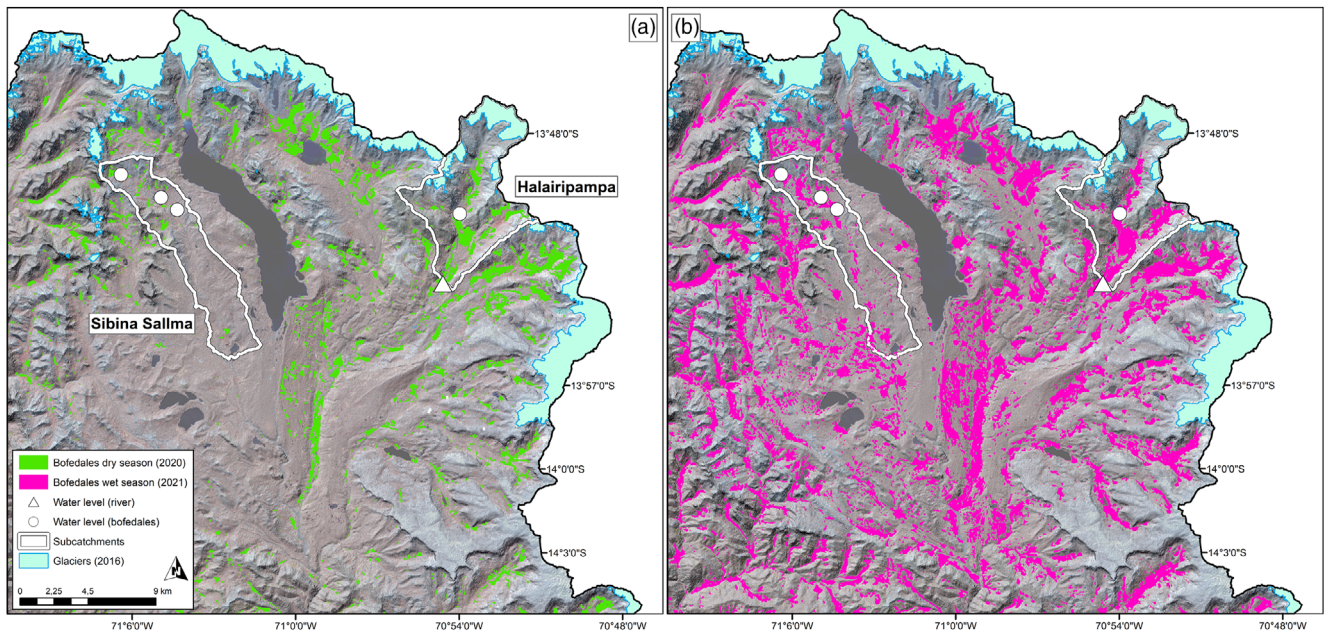
FIGURE 3 Classified bofedales extent in the region of Sibina Sallma and Halairipampa at the end of the dry season in 2020 (a) and at the end of the wet season in 2021 (b).
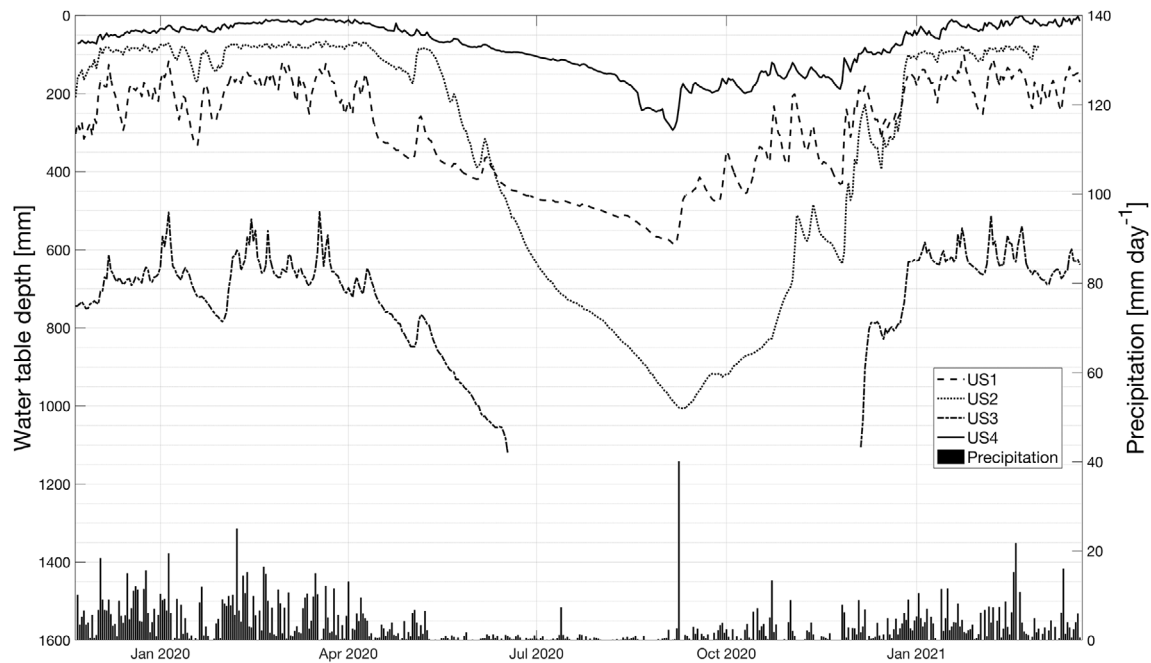

FIGURE 4 Water table observations from logger network (see Figure 1c and Table 1 for the exact locations).

and drying of small lakes has previously been described (Drenkhan et al., 2018). However, the results presented in this study are limited by the short study period focusing on one specific dry and wet season in the periods 2020–2021. More research is needed to understand the seasonal and interannual interplay of local climate (e.g., changes in the precipitation regime), morphology and deposits (e.g., stratification of permeable and impermeable layers), the role of meltwater and other surface and subsurface inputs, and human impacts in the catchments (e.g., bofedal management, irrigation and peat extraction).

3.2 | Water storage and release dynamics

3.2.1 | Water level data

All water level data reflect the strong climate seasonality (Figure 4), in line with areal bofedales extent as observed from the satellite imagery. However, some clear differences in bofedal storage behaviour can be observed. This heterogeneity is reflected in lag times obtained from the cross-correlation analysis (Table 2) and is compatible with

the findings of Cooper et al. (2019). This is not surprising because the response times of wetlands will be determined strongly by their position in the landscape, which controls both the upslope contributing area and the velocity of water release. As mentioned in the methods, US3 water levels drop below the depth of the well during the dry season and were removed from further analysis.

3.2.2 | Surface runoff production

We did not find a statistically significant correlation between bofedales extent and surface runoff production (p-value = 0.823); in fact, the fitted regression has a slightly negative trend. This is counterintuitive but may be caused by the level of hydrological connectivity. Increasing areas of disconnected wetlands may rather enhance infiltration due to improved hydraulic conductivity thereby reducing surface runoff in the catchment (Buytaert & Beven, 2011). This may act as a confounding variable for the relation, especially if it does not show a clear seasonality. However, the precipitation time series is not representative for the catchment. This is particularly noticeable during the 2020–2021 wet season, which is uncharacteristically low for the Quelccaya weather station and is not reflected in the Halairipampa discharge data (Figure 6). Furthermore, inconsistencies can be seen in the dry season where the timing of storm events in the rainfall and discharge data do not match. Differences have been attributed to localized climatic heterogeneities, which are prevalent in this region. Further exploration into the seasonality of surface runoff production would require more representative rainfall data through the installation of rainfall sensors within the catchment.

3.2.3 | Subsurface unit hydrographs

While our approach does not allow separating the hillslope release Q_H from the wetland release Q_W, the wide range of lag times (Table 2) is indicative for the diverging hydrological response of different bofedales within the catchment. The lag time of 1 day for US1 suggests a wetland that fills quickly, most likely because of overland flow and short hillslopes (Tetzlaff et al., 2014). On the other end of the spectrum US2 and US4 have lag times of around 30 days, which suggest that they are fed by a slower subsurface response, for example from longer hillslopes or deeper subsurface flow (e.g., moraines). To get further insights in the topographic and connectivity controls, we

attempted to find a relation between the lag times and topographic indices such as the upslope contributing area and soil topographic index of the bofedal locations, but this was unsuccessful, likely due to the small number of observations and the coarse resolution of the available digital elevation model.

The recession curves also show highly different behaviour (Figure 5). UH1 and UH3 drain relatively quickly, reaching half of their peak outflow in about 10 days, while UHC only drops to 50% of its peak after more than a month. This suggests that the mechanisms controlling bofedal outflow are also highly heterogeneous and may be related to processes such as the morphology of the bofedales drainage system, as well as the hydraulic conductivity, preferential flow paths and thickness of the soil mounds that separate the bofedales from the streams. Nevertheless, the unit hydrographs provide insight in the temporal dynamics of bofedales' contributions to streamflow, which can remain substantial for several months after precipitation events.

3.2.4 | Combined hydrological model

Calibrating the partitioning constants (Table 2) allows upscaling the point unit hydrographs to the catchment scale model and assessing the relative contribution of overland and subsurface flow for each of the landscape elements (Figure 6). Analysing the model simulations, we draw the following observations.

The timing of the surface runoff is roughly in line with the observed flow peaks; however, substantial errors are present, which are the direct result of the suboptimal representativity of the precipitation time series. In contrast, the simulated subsurface flow exhibits a delayed drainage of the bofedales in the dry season compared to the observations. In our model, most infiltrating rainfall flows through the unit hydrograph with the slowest response (USC; Table 2). This may be an artefact of the calibration procedure trying to compensate for errors in rainfall. Overestimation of baseflow in the dry season may also be caused by inaccurate characterization of evapotranspiration or catchment-scale losses to deep groundwater circulation. In addition, our assumption of static partitioning coefficients may be inaccurate. These could likely act more dynamically as bofedales extent and saturated area change, and bofedales may become hydrologically disconnected. Evidence of non-linear runoff response during large events where steeper hillslopes are connected due to the expansion of saturated areas has been seen in Scottish peatlands (Tetzlaff

TABLE 2 Results of the unit hydrograph analysis on the water table data.

Unit hydrograph	Logger	Lag time [days]	k [days]	n [−]	Partitioning coefficient [%]
UH1	US1	1	8.27	1.03	27.42
UHC	US2	30	12.29	3.45	68.38
	US4	32			
UH3	US3	3	3.44	2.09	4.20

Note: k, n = coefficients of the Nash (1957) distribution, partitioning coefficient = percentage of infiltrating rainfall routed through each subsurface unit hydrograph.
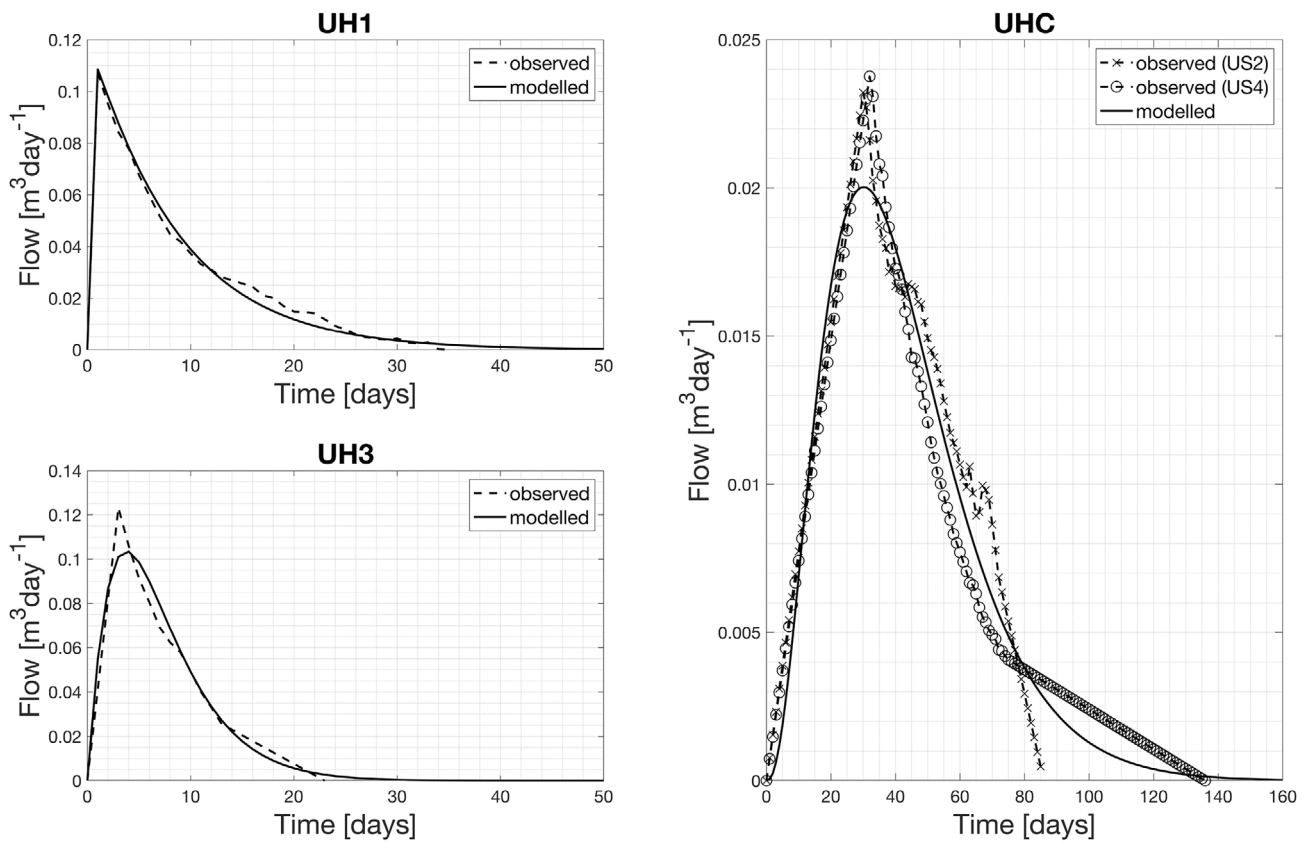
FIGURE 5 Modelled subsurface unit hydrographs fitted to observed lag times and recession curves (see Table 2 for lag times and fitted Nash (1957) coefficients).
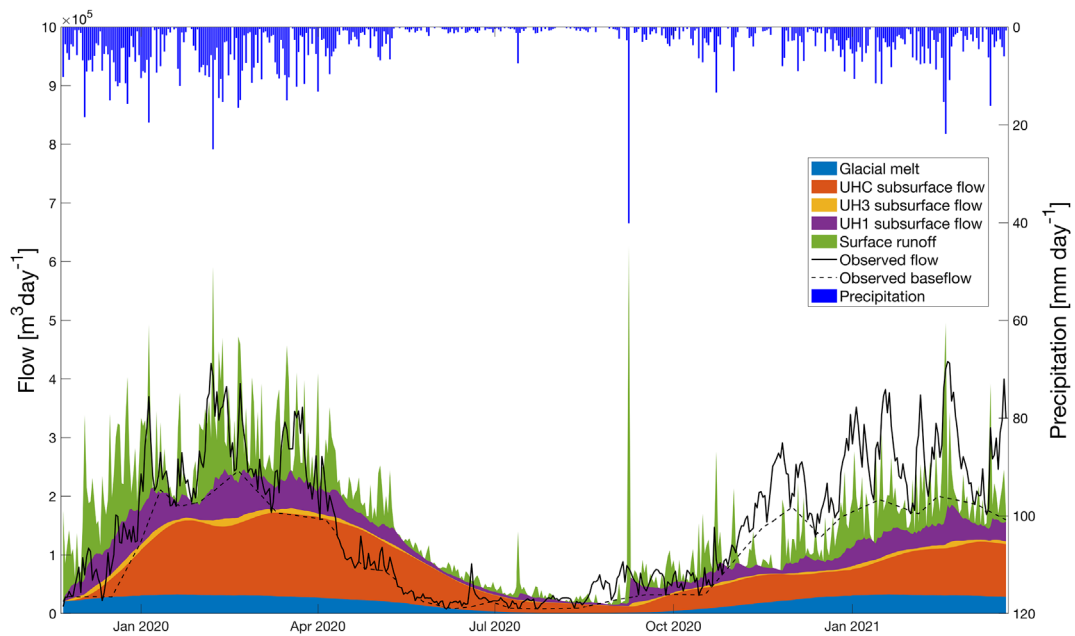

FIGURE 6 Observed and modelled discharge for Halairipampa separated by flux (glacial melt, wetland and hillslope subsurface flow, and surface runoff). Precipitation obtained from the Quelccaya glacier weather station.

et al., 2014). In Ecuadorian mountain wetlands, Buytaert and Beven (2011) highlight the importance of both non-linear and non-stationary processes caused by complex topographies and disconnected ponds

and marshes in high-Andean catchments. Further study into the dynamics of catchment area contribution and lag times during different periods (i.e., dry season, recharge period, wet season and drainage

period) combined with a more in-depth topographic, soil morphological and phytosociological study could help identify crucial relations and trends that could be used to develop a more dynamic, physically based model.

Nevertheless, our model yields some useful mechanistic understanding of the storage and release characteristics of bofedales and their role in modulating river discharge. A first observation is that glacier melt contribution is relatively low (12%), and strongly in sync with the precipitation regime. This means that streamflow during the dry season is dominated by non-glacier subsurface flow, which constitutes 74% of the total flow during the core dry season (June–August), 57% of the total flow during the core wet season (December–March) and 59% over the entire modelling period. Our results do not allow separation of the residence time of the bofedales from that of upslope contributing areas, which may consist of a combination of shallow subsurface flow and deeper flows from moraines and other geological deposits. However, the unit hydrographs show that the aggregated are substantial and can reach an order of magnitude of months.

These findings, however, are limited to the study region. Despite the wide distribution of bofedales in the VUB, challenges still lie in upscaling their relative contributions and seasonal buffering (Blöschl & Sivapalan, 1995). Adaptation strategies which prioritize natural infrastructure, such as wetland irrigation (e.g., FAO, 2022a) and restoration (e.g., FAO, 2022b) to buffer seasonally decreasing water quantity need to consider a solid evidence baseline to identify cost-effective and hydrologically most beneficial options (Drenkhan et al., 2023). For improved relevance in regional, national and international policy, it is therefore essential to develop methods that can quantify the hydrological benefits of bofedales at larger scales. This will require a better understanding of the different types of bofedales to identify representative sites for increased monitoring and subsequent development of regional hydrological models that capture the streamflow contributions of bofedales and their role within the wider basin response.

4 | CONCLUSIONS

Bofedales may provide critical water storage and seasonal buffering for Andean communities, which are increasingly important in view of the combined impacts of climate and land use changes and growing water demand in downstream areas (Drenkhan et al., 2023). In this study, we show how to estimate the storage and release characteristics of bofedales and to understand their role within the wider catchment response using a combination of remote sensing techniques and in situ hydrological monitoring of bofedal water levels, precipitation and streamflow. Applying our methodology to the Vilcanota-Urubamba basin, we find a strong seasonal variation in bofedales' water storage at both the sub-catchment and wider river basin scale. We applied the linear reservoir concept to bofedal water levels to estimate unit hydrographs for representative bofedales. The large differences in the residence time of these unit hydrographs (1–30 days) suggest a strong heterogeneity in

subsurface storage and release behaviour between bofedales, which we attribute to hydrological connectivity and upslope contributing area. Upscaling these hydrographs to the catchment scale by means of calibrated contribution factors allowed estimating the contribution of different end members (glacier melt, surface runoff and combined hillslope and bofedal subsurface outflow). We find that non-glacier subsurface flow is substantial (59% of total streamflow over the entire modelling period) and is sustained for several months after precipitation events (74% of core dry season streamflow). This highlights the importance of considering bofedales in local water management strategies including nature-based solutions. It also illustrates the need to base catchment interventions on a solid evidence baseline that identifies the specific hydrological conditions and benefits of high-altitude wetlands to counteract decreasing water availability. Improved monitoring in representative bofedal sites is, therefore, crucial to enable upscaling our hydrological understanding for relevance in regional, national and international policy.

CONFLICT OF INTEREST STATEMENT
The authors declare that there is no conflict of interest.

DATA AVAILABILITY STATEMENT
- Glacier and bofedales extent in Figure 1: data available upon request.
- Sibinacocha Lake weather station data: provided by SENAMHI, available at https://www.senamhi.gob.pe/?p=estaciones
- Quelccaya Glacier weather station data: provided by SENAMHI in collaboration with UNSAAC and Appalachian State University, available at https://climate.appstate.edu/Data/Met/Peru/Quelccaya/
- Bofedal water levels and Halairipampa discharge data from in situ network of loggers: available upon request.
- Input data and results from the glacial melt model: available upon request.
- Results from the bofedal classification: available upon request.

ORCID

Anthony C. Ross https://orcid.org/0000-0003-3106-8131

Marc Martinez Mendoza https://orcid.org/0009-0000-4152-5389

Fabian Drenkhan https://orcid.org/0000-0002-9443-9596

Nilton Montoya https://orcid.org/0000-0002-4147-2579

Jan R. Baiker https://orcid.org/0000-0002-2634-0690

Jonathan D. Mackay https://orcid.org/0000-0003-4373-5747

David M. Hannah https://orcid.org/0000-0003-1714-1240

Wouter Buytaert https://orcid.org/0000-0001-6994-4454

REFERENCES

Alcántara-Boñón, G. H. (2014). Eco-systemic services in Cajamarca region. *Espacio Y Desarrollo*, *26*, 75–97. https://revistas.pucp.edu.pe/index.php/espacioydesarrollo/article/view/13967

Anderson, T. G., Christie, D. A., Chávez, R. O., Olea, M., & Anchukaitis, K. J. (2021). Spatiotemporal peatland productivity and climate relationships across the Western south American altiplano. *Journal of Geophysical Research – Biogeosciences*, *126*(6), e2020JG005994. https://doi.org/10.1029/2020JG005994

Baum, F., & Zanetti, M. (2015). Streamlined generalization tool for planetary surface mapping using ArcGIS ModelBuilder software on multi-spectral datasets. 46th Lunar and Planetary Science Conference. https://www.hou.usra.edu/meetings/lpsc2015/pdf/1233.pdf

Belgiu, M., & Drăguţ, L. (2016). Random forest in remote sensing: A review of applications and future directions. *ISPRS Journal of Photogrammetry and Remote Sensing*, *114*, 24–31. https://doi.org/10.1016/j.isprsjprs.2016.01.011

Blöschl, G., & Sivapalan, M. (1995). Scale issues in hydrological modelling: A review. *Hydrological Processes*, *9*(3–4), 251–290. https://doi.org/10.1002/hyp.3360090305

Buckley, S. M., Agram, P. S., Belz, J. E., Crippen, R. E., Gurrola, E. M., Hensley, S., Kobrick, M., Lavalle, M., Martin, J. M., Neumann, M., Nguyen, Q. D., Rosen, P. A., Shimada, J. D., Simard, M., & Tung, W. W. (2020). NASADEM: User Guide. https://lpdaac.usgs.gov/documents/592/NASADEM_User_Guide_V1.pdf

Buitrón-Aliaga, C., & Fernández-Callisaya, J. (2012). *Estudio espacial multitemporal de variaciones en superficie observadas a través de imágenes satelitales Landsat en una región del Parque Nacional Sajama*. La Paz. https://www.weadapt.org/sites/weadapt.org/files/2017/november/estudio_espacial_multitemporal_de_variaciones_en_superficie.pdf

Buytaert, W., & Beven, K. (2011). Models as multiple working hypotheses: Hydrological simulation of tropical alpine wetlands. *Hydrological Processes*, *25*(11), 1784–1799. https://doi.org/10.1002/hyp.7936

Buytaert, W., de Bièvre, B., Wyseure, G., & Deckers, J. (2004). The use of the linear reservoir concept to quantify the impact of changes in land use on the hydrology of catchments in the Andes. *Hydrological Earth Systems Science*, *8*(1), 108–114. https://doi.org/10.5194/hess-8-108-2004

Castellanos, E., Lemos, M., Astigarraga, L., Chacón, N., Cuvi, N., Huggel, C., Miranda, L., Vale, M., Ometto, J., Peri, P., Postigo, J., Ramajo, L., Roco, L., Rusticucci, M., Menezes, J., Borges, P., Bueno, J., Cuesta, F., Drenkhan, F., & Valladares, M. (2022). *IPCC 2022. WGII sixth assessment report* (pp. 1–181). Central and South America.

Chicco, D., Warrens, M. J., & Jurman, G. (2021). The Matthews correlation coefficient (MCC) is more informative than Cohen's kappa and brier score in binary classification assessment. *IEEE Access*, *9*, 78368–78381. https://doi.org/10.1109/ACCESS.2021.3084050

Chimner, R. A., Bourgeau-Chavez, L., Grelik, S., Hribljan, J. A., Clarke, A. M. P., Polk, M. H., Lilleskov, E. A., & Fuentealba, B. (2019). Mapping Mountain peatlands and wet meadows using multi-date, multi-sensor remote sensing in the cordillera Blanca, Peru. *Wetlands*, *39*(5), 1057–1067. https://doi.org/10.1007/s13157-019-01134-1

Cochran, W. G. (1977). *Sampling techniques* (3rd ed.). Wiley.

Cooper, D. J., Sueltenfuss, J., Oyague, E., Yager, K., Slayback, D., Caballero, E. M., Argollo, J., & Mark, B. G. (2019). Drivers of peatland water table dynamics in the Central Andes, Bolivia and Peru. *Hydrological Processes*, *33*(13), 1913–1925. https://doi.org/10.1002/hyp.13446

Dangles, O., Rabatel, A., Kraemer, M., Zeballos, G., Soruco, A., Jacobsen, D., & Anthelme, F. (2017). Ecosystem sentinels for climate change? Evidence of wetland cover changes over the last 30 years in the tropical Andes. *PLoS One*, *12*(5), e0175814. https://doi.org/10.1371/journal.pone.0175814

Drenkhan, F., Buytaert, W., Mackay, J. D., Barrand, N. E., Hannah, D. M., & Huggel, C. (2023). Looking beyond glaciers to understand mountain water security. *Nature Sustainability.*, *6*(2), 130–138. https://doi.org/10.1038/s41893-022-00996-4

Drenkhan, F., Guardamino, L., Huggel, C., & Frey, H. (2018). Current and future glacier and lake assessment in the deglaciating Vilcanota-Urubamba basin, Peruvian Andes. *Global and Planetary Change*, *169*, 105–118. https://doi.org/10.1016/j.gloplacha.2018.07.005

Dussaillant, I., Berthier, E., Brun, F., Masiokas, M., Hugonnet, R., Favier, V., Rabatel, A., Pitte, P., & Ruiz, L. (2019). Two decades of glacier mass loss along the Andes. *Nature Geoscience*, *12*(10), 802–808. https://doi.org/10.1038/s41561-019-0432-5

Earle, L. R., Warner, B. G., & Aravena, R. (2003). Rapid development of an unusual peat-accumulating ecosystem in the Chilean altiplano. *Quaternary Research*, *59*(1), 2–11. https://doi.org/10.1016/S0033-5894(02)00011-X

Erwin, K. L. (2008). Wetlands and global climate change: The role of wetland restoration in a changing world. *Wetlands Ecology and Management*, *17*, 71–84. https://doi.org/10.1007/s11273-008-9119-1

FAO. (2022a). Ampliación del área de bofedales para criar alpacas en Chalhuanca, Perú. Casos de gestión de turberas. Organización de las Naciones Unidas para la Alimentación y la Agricultura - FAO. https://www.fao.org/3/cc0993es/cc0993es.pdf

FAO. (2022b). Restauración hidrológica de bofedales en el Parque Nacional Huascarán. Casos de gestión de turberas. Organización de las Naciones Unidas para la Alimentación y la Agricultura - FAO. https://www.fao.org/3/cc2292es/cc2292es.pdf

Fyffe, C. L., Potter, E., Fugger, S., Orr, A., Fatichi, S., Loarte, E., Medina, K., Hellström, R. Å., Bernat, M., Aubry-Wake, C., Gurgiser, W., Perry, L. B., Suarez, W., Quincey, D. J., & Pellicciotti, F. (2021). The energy and mass balance of Peruvian glaciers. *Journal of Geophysical Research-Atmospheres*, *126*(23), e2021JD034911. https://doi.org/10.1029/2021JD034911

Gandarillas, R. V., Jiang, Y., & Irvine, K. (2016). Assessing the services of high mountain wetlands in tropical Andes: A case study of Caripe wetlands at Bolivian altiplano. *Ecosystem Services*, *19*, 51–64. https://doi.org/10.1016/j.ecoser.2016.04.006

Garcia Dulanto, J. L. (2018). *Implementación de una metodología para la identificación de bofedales usando datos imágenes satelitales Landsat - caso estudio: bofedal Chunal, cuenca alta del río Chillón.* (pp. 1–195). *Master's thesis*. Universidad Nacional Mayor de san Marcos. https://cybertesis.unmsm.edu.pe/handle/20.500.12672/10446

García, E., & Beck, S. G. (2006). Puna. In M. Moraes, B. Øllgaard, L. P. Kvist, F. Borchsenius, & H. Balslev (Eds.), *Botánica económica de los Andes Centrales* (pp. 51–76). Bolivia, Universidad Mayor de San Andrés.

García, E., & Lleellish, M. A. (2012). Cartografiado de bofedales usando imágenes de satellite Landsat en una cuenca altoandina del Perú. *Revista de Teledetección*, *38*, 92–108. http://www.aet.org.es/revistas/revista38/Numero38_09.pdf

Garcia, E., & Otto, M. (2015). Caracterización ecohidrológica de humedales alto andinos usando imágenes de satélite multitemporales en la cabecera de cuenca del Río Santa, Ancash, Perú. *Ecología Aplicada*, *14*(2), 115–125. http://www.scielo.org.pe/scielo.php?pid=S1726-22162015000200004&script=sci_abstract

Gatti, A., & Bertolini, A. (2015). Sentinel-2 products specification document. https://sentinel.esa.int/documents/247904/349490/s2_msi_product_specification.pdf

Glas, R., Lautz, L., McKenzie, J., Mark, B., Baraer, M., Chavez, D., & Maharaj, L. (2018). A review of the current state of knowledge of proglacial hydrogeology in the cordillera Blanca, Peru. WIREs Water, 5(5), e1299. https://doi.org/10.1002/wat2.1299

Gustard, A., Bullock, A., & Dixon, J. M. (1992). Low flow estimation in the United Kingdom. Wallingford https://nora.nerc.ac.uk/id/eprint/6050/1/IH_108.pdf

Ham, J., Chen, Y., Crawford, M. M., & Ghosh, J. (2005). Investigation of the random forest framework for classification of hyperspectral data. IEEE Transactions on Geoscience and Remote Sensing, 43(3), 492–501. https://doi.org/10.1109/TGRS.2004.842481

Hribljan, J. A., Suarez, E., Bourgeau-Chavez, L., Endres, S., Lilleskov, E. A., Chimbolema, S., Wayson, C., Serocki, E., & Chimner, R. A. (2017). Multidate, multisensor remote sensing reveals high density of carbon-rich mountain peatlands in the páramo of Ecuador. Global Change Biology, 23(12), 5412–5425. https://doi.org/10.1111/gcb.13807

Jara, C., Delegido, J., Ayala, J., Lozano, P., Armas, A., & Flores, V. (2019). Estudio de bofedales en los Andes ecuatorianos a través de la comparación de imágenes Landsat-8 y Sentinel-2. Revista De Teledetección, 53, 45–57. https://doi.org/10.4995/raet.2019.11715

Kumar, R. (2020). Automated Field Boundary Detection Using Modern Machine Learning Techniques. https://lib.dr.iastate.edu/creativecomponents/555

Lazo, P. X., Mosquera, G. M., McDonnell, J. J., & Crespo, P. (2019). The role of vegetation, soils, and precipitation on water storage and hydrological services in Andean Páramo catchments. Journal of Hydrology, 572, 805–819. https://doi.org/10.1016/j.jhydrol.2019.03.050

Li, C., Zhou, L., & Xu, W. (2021). Estimating aboveground biomass using sentinel-2 msi data and ensemble algorithms for grassland in the shengjin lake wetland, China. Remote Sensing, 13(8), 1595. https://doi.org/10.3390/rs13081595

Mahdavi, S., Salehi, B., Granger, J., Amani, M., Brisco, B., & Huang, W. (2018). Remote sensing for wetland classification: A comprehensive review. GIScience & Remote Sensing, 55(5), 623–658. https://doi.org/10.1080/15481603.2017.1419602

Maldonado Fonkén, M. S. (2014). An introduction to the bofedales of the Peruvian high Andes. Mires and Peat, 15, 1–13. http://mires-and-peat.net/media/map15/map_15_05.pdf

Mango-Mamani, B. C. (2017). Valoración económica de los servicios ecosistémicos de regulación, de los bofedales del centro poblado de Chalhuanca, distrito de Yanque, provincia de Caylloma, región Arequipa. Universidad Nacional San Agustín de Arequipa.

Maussion, F., Butenko, A., Champollion, N., Dusch, M., Eis, J., Fourteau, K., Gregor, P., Jarosch, A. H., Landmann, J., Oesterle, F., Recinos, B., Rothenpieler, T., Vlug, A., Wild, C. T., & Marzeion, B. (2019). The open global glacier model (OGGM) v1.1. Geoscientific Model Development, 12(3), 909–931. https://doi.org/10.5194/gmd-12-909-2019

Meneses, R., Domic, A., Beck, S., & Yager, K. (2019). Bofedales Altoandinos: Un Oasis en la Puna.

Miguel, B., Edell, A., Edson, Y., & Edwin, P. (2012). A phytoremediation approach using Calamagrostis ligulata and Juncus imbricatus in Andean wetlands of Peru. Environmental Monitoring and Assessment, 185, 323–334. https://doi.org/10.1007/s10661-012-2552-x

MINAM. (2019). Guía de evaluación del estado del ecosistema de bofedal. https://sinia.minam.gob.pe/documentos/guia-evaluacion-estado-ecosistema-bofedal

Mohammadi, A., Kamran, K. V., Karimzadeh, S., Shahabi, H., & Al-Ansari, N. (2020). Flood detection and susceptibility mapping using Sentinel-1 time series, alternating decision trees, and bag-ADTree models. Complexity, 2020, 1–21. https://doi.org/10.1155/2020/4271376

Monge-Salazar, M. J., Tovar, C., Cuadros-Adriazola, J., Baiker, J. R., Montesinos-Tubée, D. B., Bonnesoeur, V., Antiporta, J., Román-Dañobeytia, F., Fuentealba, B., Ochoa-Tocachi, B. F., & Buytaert, W.

(2022). Ecohydrology and ecosystem services of a natural and an artificial bofedal wetland in the Central Andes. The Science of the Total Environment, 838, 155968. https://doi.org/10.1016/j.scitotenv.2022.155968

Mosquera, G. M., Célleri, R., Lazo, P. X., Vaché, K. B., Perakis, S. S., & Crespo, P. (2016). Combined use of isotopic and hydrometric data to conceptualize ecohydrological processes in a high-elevation tropical ecosystem. Hydrological Processes, 30(17), 2930–2947. https://doi.org/10.1002/hyp.10927

Mosquera, G. M., Lazo, P. X., Célleri, R., Wilcox, B. P., & Crespo, P. (2015). Runoff from tropical alpine grasslands increases with areal extent of wetlands. Catena, 125, 120–128. https://doi.org/10.1016/j.catena.2014.10.010

Mutanga, O., & Kumar, L. (2019). Google Earth Engine Applications. Remote Sensing, 11(5), 591. https://doi.org/10.3390/rs11050591

Nash, J. E. (1957). The form of the instantaneous unit hydrograph. International Association of Hydrological Sciences., 45, 114–121.

Navarro, G., MacDonell, S., & Valois, R. (2023). A conceptual hydrological model of semiarid Andean headwater systems in Chile. Progress in Physical Geography: Earth and Environment, 030913332211476. https://doi.org/10.1177/03091333221147649

Nelder, J. A., & Mead, R. (1965). A simplex method for function minimization. The Computer Journal, 7(4), 308–313. https://doi.org/10.1093/comjnl/7.4.308

Neukom, R., Rohrer, M., Calanca, P., Salzmann, N., Huggel, C., Acuña, D., Christie, D. A., & Morales, M. S. (2015). Facing unprecedented drying of the Central Andes? Precipitation variability over the period AD 1000–2100. Environmental Research Letters, 10(8), 084017. https://doi.org/10.1088/1748-9326/10/8/084017

Olofsson, P., Foody, G. M., Herold, M., Stehman, S. V., Woodcock, C. E., & Wulder, M. A. (2014). Good practices for estimating area and assessing accuracy of land change. Remote Sensing of Environment, 148, 42–57. https://doi.org/10.1016/j.rse.2014.02.015

Otto, M., & Gibbons, R. E. (2017). Potential effects of projected decrease in annual rainfall on spatial distribution of high Andean wetlands in southern Peru. Wetlands, 37(4), 647–659. https://doi.org/10.1007/s13157-017-0896-2

Otto, M., Scherer, D., & Richters, J. (2011). Hydrological differentiation and spatial distribution of high altitude wetlands in a semi-arid Andean region derived from satellite data. Hydrology and Earth System Sciences, 15(5), 1713–1727. https://doi.org/10.5194/hess-15-1713-2011

Polk, M. H., Young, K. R., Baraer, M., Mark, B. G., McKenzie, J. M., Bury, J., & Carey, M. (2017). Exploring hydrologic connections between tropical mountain wetlands and glacier recession in Peru's cordillera Blanca. Applied Geography, 78, 94–103. https://doi.org/10.1016/j.apgeog.2016.11.004

Rodríguez-Morales, M., Acevedo-Novoa, D., Machado, D., Ablan, M., Dugarte, W., & Dávila, F. (2019). Ecohydrology of the Venezuelan páramo: Water balance of a high Andean watershed. Plant Ecology and Diversity, 12(6), 573–591. https://doi.org/10.1080/17550874.2019.1673494

Seneviratne, S., Nicholls, N., Easterling, D., Goodess, C., Kanae, S., Kossin, J., Luo, Y., Marengo, J., McInnes, K., Rahimi, M., Reichstein, M., Sorteberg, A., Vera, C., Zhang, X., Alexander, L. V., Allen, S., Benito, G., Cavazos, T., Clague, J., … Zwiers, F. W. (2012). Changes in Climate Extremes and their Impacts on the Natural Physical Environment. https://doi.org/10.7916/d8-6nbt-s431

Shamsoddini, A., & Raval, S. (2018). Mapping red edge-based vegetation health indicators using Landsat TM data for Australian native vegetation cover. Earth Science Informatics, 11(4), 545–552. https://doi.org/10.1007/s12145-018-0347-5

Shannon, S., Smith, R., Wiltshire, A., Payne, T., Huss, M., Betts, R., Caesar, J., Koutroulis, A., Jones, D., & Harrison, S. (2019). Global glacier volume projections under high-end climate change scenarios. The Cryosphere, 13(1), 325–350. https://doi.org/10.5194/tc-13-325-2019

Shepherd, J. D., Schindler, J., & Dymond, J. R. (2020). Automated mosaicking of Sentinel-2 satellite imagery. *Remote Sensing*, *12*(22), 3680. https://doi.org/10.3390/rs12223680

Somers, L. D., & McKenzie, J. M. (2020). A review of groundwater in high mountain environments. *WIREs Water*, *7*(6), e1475. https://doi.org/10.1002/wat2.1475

Soulsby, C., Tetzlaff, D., & Hrachowitz, M. (2009). Tracers and transit times: Windows for viewing catchment scale storage? *Hydrological Processes*, *23*(24), 3503–3507. https://doi.org/10.1002/hyp.7501

Squeo, F. A., Warner, B. G., Aravena, R., & Espinoza, D. (2006). Bofedales: High altitude peatlands of the Central Andes. *Revista Chilena De Historia Natural*, *79*(2), 245–255.

Starovoitov, V. V., & Golub, Y. I. (2020). Comparative study of quality estimation of binary classification. *Informatics*, *17*(1), 87–101. https://doi.org/10.37661/1816-0301-2020-17-1-87-101

Tetzlaff, D., Birkel, C., Dick, J., Geris, J., & Soulsby, C. (2014). Storage dynamics in hydropedological units control hillslope connectivity, runoff generation, and the evolution of catchment transit time distributions. *Water Resources Research*, *50*(2), 969–985. https://doi.org/10.1002/2013WR014147

UNEP. (2022). Global Peatlands Assessment: The State of the World's Peatlands. https://www.unep.org/resources/global-peatlands-assessment-2022

Valois, R., Araya Vargas, J., MacDonell, S., Guzman Pinones, C., Fernandoy, F., Yanez Carrizo, G., Cuevas, J. G., Sproles, E. A., & Maldonado, A. (2021). Improving the underground structural characterization and hydrological functioning of an Andean peatland using geoelectrics and water stable isotopes in semi-arid Chile. *Environment and Earth Science*, *80*(1), 41. https://doi.org/10.1007/s12665-020-09331-6

Valois, R., Schaffer, N., Figueroa, R., Maldonado, A., Yáñez, E., Hevia, A., Yánez Carrizo, G., & MacDonell, S. (2020). Characterizing the water storage capacity and hydrological role of mountain peatlands in the arid Andes of north-Central Chile. *Water*, *12*(4), 1071. https://doi.org/10.3390/w12041071

White-Nockleby, C., Prieto, M., Yager, K., & Meneses, R. I. (2021). Understanding Bofedales as cultural landscapes in the Central Andes. *Wetlands*, *41*(8), 102. https://doi.org/10.1007/s13157-021-01500-y

Yager, K., Valdivia, C., Slayback, D., Jimenez, E., Meneses, R., Palabral-Aguilera, A., Bracho, M., Romero, D., Hubbard, A., Pacheco, P., Calle, A., Alberto, H., Yana, O., Ulloa, D., Zeballos, G., & Romero, A. (2019). Socio-ecological dimensions of Andean pastoral landscape change: Bridging traditional ecological knowledge and satellite image analysis in Sajama National Park, Bolivia. *Regional Environmental Change*, *19*, 1353–1369. https://doi.org/10.1007/s10113-019-01466-y

SUPPORTING INFORMATION

Additional supporting information can be found online in the Supporting Information section at the end of this article.